Title. C5 Methylation Confers Accessibility, Stability and Selectivity to Picrotoxinin

Guanghu Tong,[1] Samantha Griffin,[2] Avery Sader,[2] Anna B. Crowell,[3] Ken Beavers,[2] Jerry Watson,[2] Zachary Buchan,[2] Shuming Chen,[3,*] Ryan A. Shenvi[1,*]

Affiliations: [1]Department of Chemistry, Scripps Research, 10550 North Torrey Pines Road, La Jolla, California 92037, United States.

[2]Corteva Agriscience, 9330 Zionsville Road, Indianapolis, Indiana 46268, United States.

[3]Department of Chemistry and Biochemistry, Oberlin College, 119 Woodland Street, Oberlin, Ohio 44074, United States.

[*]Correspondence to: shuming.chen@oberlin.edu, rshenvi@scripps.edu

Summary Paragraph. Natural product total synthesis enables gain of function through deep-seated modification of structure.[1] Synthetic difficulty can, however, obstruct meaningful optimization campaigns. To simplify access, the complexity of the target (TGT) can be lowered—a strategy described within function-oriented synthesis.[2] Alternatively, the chemical space immediately surrounding the TGT can be searched for analogs of equal or greater complexity that also simplify access.[3] This strategy—dynamic retrosynthetic analysis—maintains most physicochemical properties of the TGT (locus in chemical space) but opens new synthetic paths unavailable to the natural product itself and can provide functional advantage.[3,4,14] Here we experimentally interrogate these ideas by generation of two parallel series of picrotoxinin (PXN) analogs to identify leads with ligand-gated ion channel (LGIC) selectivity. One series derives from PXN via semi-synthesis, and the other from 5MePXN via total synthesis. Methylation at C5 decreases potency against vertebrate ion channels ($GABA_A$ receptors) but maintains or increases antagonism of homologous invertebrate GABA-gated chloride channels (RDL receptors). Optimal 5MePXN analogs appear to change the PXN binding pose within $GABA_A$Rs by disruption of a hydrogen bond network. The C5 methyl also stabilizes the scaffold substantially against irreversible C15 solvolysis by destabilizing an intermediate twist-boat conformer, which returns to 5MePXN instead of progressing to degradant. These discoveries are made possible by the lower synthetic burden of 5MePXN and are illuminated by the parallel analog series, which allows unambiguous identification of the role of the synthetically simplifying C5 methyl. Rapid access to functionally-privileged analogs by TGT point mutation underscores the value of dynamic retrosynthetic analysis as a problem-solving heuristic.

Body. Seeds of *Anamerta cocculus* have for centuries featured as poisons[5] due to their content of picrotoxinin (PXN),[6] a sesquiterpene that rapidly absorbs, penetrates the brain and potently antagonizes $GABA_A$ receptors.[7] PXN can be isolated with ease as picrotoxin[5] (PTX)—a 1:1 mixture with the less-active congener picrotin (PTN)[8]—and has become a widespread tool in neuroscience to identify and/or ablate GABAergic signaling.[9] Mammalian $GABA_A$ receptors are inhibitory ligand-gated ion channels (LGICs), which form an extensive phylogenetic tree of membrane-bound pentameric protein complexes.[10] Despite the widespread availability of PXN, no semi-synthetic analogs have demonstrated improved properties: selectivity among LGICs or stability to degradation.[6] PXN is surprisingly unstable. Rapid and irreversible solvolysis occurs with 5 mol% sodium methoxide in methanol[11] or 1% sulfuric acid in water.[12] Reversible solvolysis occurs in pH 7–9 water,[13a] pH 7.4 buffer (half-life ~ 45 minutes) or mouse plasma (half-life ~ 1 h, vide infra).[13b] In each case, the degradation products are weakly active or inactive in vivo.[13,7b] Total synthesis might solve these problems with skeletal changes that stabilize the scaffold and allow diversification. However, no syntheses have delivered analogs for assay against LGICs, let alone selectivity among LGICs, or stability to solvolysis.

Recently, we reported a short synthesis of PXN that identified a retrosynthetic methylation transform to control stereochemistry and conformation of early intermediates.[14] Whereas excision of this extra methyl required multiple steps, retention of the methyl allowed a more rapid and higher-yielding entry into PXN chemical space (PXN: 13 steps, 0.6% overall vs. 5MePXN: 9 steps, 8% overall). 5MePXN retained binding to rat $GABA_A$ receptors and we wondered if, beyond this proof-of-principle, the synthetic platform might provide a means to perturb selectivity among LGICs. Here we show that the total synthesis of 5MePXN allows, for the first time, diversification of the PXN scaffold, optimization of selectivity between mammalian $GABA_A$ and insect RDL receptors, and a remarkable stabilization of the PXN scaffold to both strong acid and strong base.

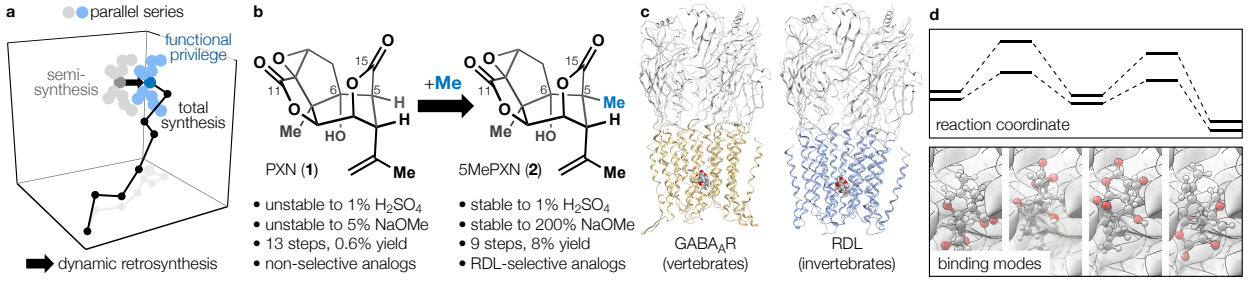

Fig. 1. Overview of this work: target modification to explore functionally privileged chemical space. a, Exploration of parallel series to explore the effects of a scaffold uniquely accessible through dynamic retrosynthetic analysis / total synthesis. **b,** C5 methylation increases stability to base and acid, increases yield, decreases required steps and increases receptor selectivity. **c,** Assay against $GABA_A$ and RDL receptors, representative of vertebrate (e.g. human) and invertebrate (e.g. insect) ligand-gated ion channels (LGICs), respectively. Left: rat $GABA_A$ homology model from PDB 6X40 template with sequence from *R. norvegicus,* gold). Right: fly RDL homology model from PDB 6X40 template with sequence from *D. melanogaster,* blue). **d,** Computational analyses provide models for increased stability and selectivity of the 5MePXN series.

The 5 rings, 8 stereocenters and 6 oxygens of PXN comprise a Böttcher complexity (C_m) of 467.61 mcbits packaged into 229 $Å^3$, to give a density of 2.04 mcbits/$Å^3$. Its small volume allows PXN to fit into the narrow space near the desensitization gate[15] of $GABA_A$ receptors (largest pore radius *ca.* 3Å in α1β3γ2L).[16] Methylation of C5 maintains the C_m (480.1 mcbits, +3%), the ligand volume (247 $Å^3$, +6%) and the information density (1.96 mcbits/$Å^3$, -4%), and appears to access a hydrophobic pocket defined by residues L259/ T256 (β3 subunit) and T261 (α1 subunit).[16,17] In a preliminary screen, we found that 5MePXN competed with [^{3}H]TBOB for binding to rat cerebral cortex with an IC_{50} of 2.1 ± 0.3 μM,[18] corresponding to a 10-fold loss in potency from PXN. We wondered if this potency loss at mammalian receptors could serve as an advantage if the 5Me series bound invertebrate receptors with greater affinity, broadening the selectivity index of PXN analogs between mammals and insects.

The high oxidation state, lack of modifiable functional groups and complex structure of PXN obstructed functionalization in prior studies.[6] Moreover, interactions between PXN and $GABA_A$ receptor in the narrow pore do not allow expansive derivatization of the PXN scaffold: e.g. acylation of the C6 hydroxyl or C15 bridge lactone opening ablates binding.[6] Thus, we pursued analog design that 1) minimized volume and conformational changes using single atom replacements,[1] 2) probed lipophilic modification at C12 to avoid the reported inactivity of PTN (see Figure 2) at RDL,[25] and 3) explored hydrogen bond network disruption (de-epoxidation, hydroxylation or fluorination[25]). The divergent syntheses of parallel PXN and 5MePXN analogs are shown in Figure 2. Diversification of the 5Me series began from late-stage intermediate **7**, 2.7 grams of which were accessed in a single-pass scale up over 6 steps from dimethylcarvone (**3**) in 27% overall yield. Oxidation of the

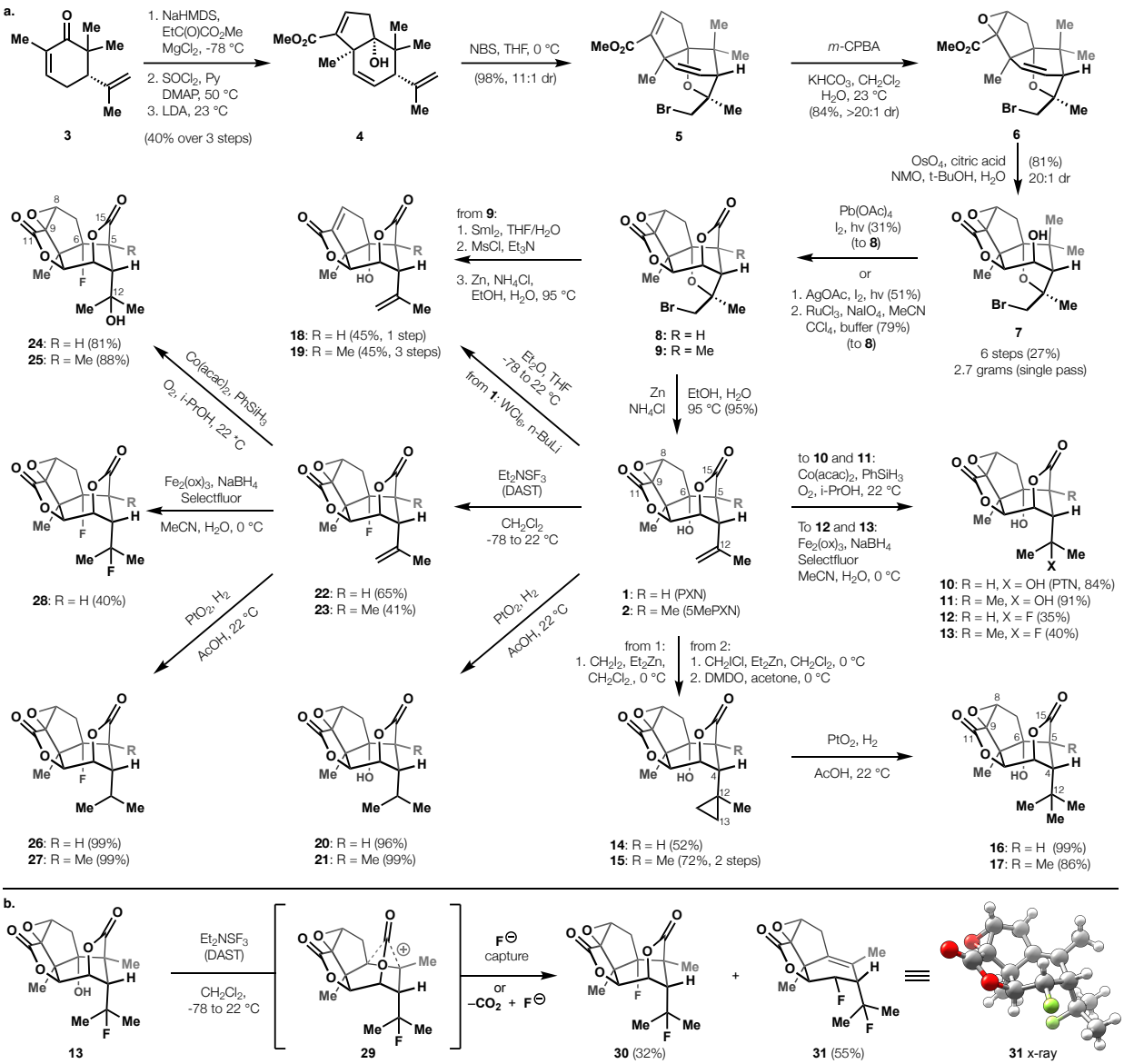

Fig. 2. **Parallel diversification of PXN and 5MePXN**. **a,** Analogs probe oxygenation and fluorination patterns. **b,** C5-methylation affects reactivity in unexpected ways (see also Figure 3).

gem-dimethyl motif to the bridging lactone could be carried out in one step ($Pb(OAc)_4$, I_2, 31%) or two steps (AgOAc, I_2, 51%; $RuCl_3$, $NaIO_4$, 79%). The formation of 5-Me-picrotin (**11**) was accomplished in excellent yield (81%) according to our previous synthesis of picrotin (**10**) using Mukaiyama hydration.[19,14] 12-F PXN **12** and 12F-5MePXN **13** were synthesized through the highly effective Boger hydrofluorination (35% and 40% yield, respectively).[20] The C12/ C13 cyclopropane was introduced on picrotoxinin scaffold through Simmons–Smith cyclopropanation (CH_2I_2, Et_2Zn) to furnish **14** in modest yield (52%). Under the same conditions, 5MePXN yielded the desired product in less than 5% yield, but an alternative procedure was developed using CH_2ICl,[21] which resulted in a 1:3 mixture of cyclopropane 5MePXN **15** and 8,9-deoxy cyclopropane-5MePXN (see SI). Fortunately, treatment of this mixture with freshly prepared dimethyldioxirane (DMDO) converted 8,9-deoxy-cyclopropane-5MePXN to **15** in 72% yield (two steps). Cyclopropanation at C12/13 not only delivered **14** and **15** but also allowed us to prepare C4 *tert*-butyl analogs. Whereas verified $GABA_AR$ antagonists like bilobalide, TBPS and TBOB

contain a *tert*-butyl group,[22] analogous PXN substitution has not been assayed but the isosteric tertiary alcohol PTN (**10**) significantly reduces binding affinity. Two hydromethylation methods were attempted on **1** and **2**,[23] but only hydrogenation of corresponding cyclopropane (**14** and **15**) with 50 mol% Adam's catalyst (PtO_2) yielded **16** and **17**, in 99% and 86% yield, respectively. Degradation product 8,9-deoxyPXN (**18**) was accessed according to Trost's method (WCl_6, *n*-BuLi, 45% yield).[24] The corresponding 5Me analog was accessed by exposure of 5MeBrPXN **9** to samarium diiodide (SmI_2) in degassed THF/H_2O (20:1, v:v), which led to chemoselective epoxide opening without reducing the primary bromide. Elimination (MsCl, Et_3N) yielded 8,9-deoxy-5Me-BrPXN, which was then heated under reductive debromination conditions (Zn, NH_4Cl, 95 °C) to deliver **19** in 45% yield over three steps. DihydroPXN **20**, another natural $GABA_AR$ antagonist, could be conveniently obtained from PXN through hydrogenation (PtO_2, 96% yield); dihydro 5-methyl-PXN **21** was prepared in a similar manner in quantitative yield.

Hydration of the $\Delta^{12,13}$-alkene (PXN to PTN) dramatically reduced binding affinity to $GABA_A$ receptors[6] but not RDL (see below). We wondered whether replacement of one or both C12 and C6 hydroxyls with fluorine might disrupt internal hydrogen bonding and, combined with C5 methylation, differentially affect affinity for LGIC receptors. Advanced synthetic intermediate 6FPXN **22** was prepared from **1** (65% yield) by reaction with diethylaminosulfur trifluoride (DAST),[25] and further employed as starting material for the synthesis of analogues 6F-picrotin **24** and 6F-dihydroPXN **26**. In parallel, analogous derivatives of 6F-5MePXN **23** were synthesized in 41% yield. Cobalt catalyzed $\Delta^{12,13}$-alkene hydration smoothly proceeded on 6F-PXN and 6F-5MePXN, delivering **24** and **25** in 81% and 88% yield, respectively. Dihydro-congeners **26** and **27** were prepared as above using PtO_2-catalyzed hydrogenation.

6,12-DifluoroPXN **28** arose via Boger hydrofluorination ($Fe_2(ox)_3$, Selectfluor, $NaBH_4$) in 40% yield (accompanying alkene reduction byproduct) but confounded assignment due to an unexpected, strong fluorine-fluorine coupling by ^{19}F NMR ($J_{F,F}$ = 31.2 Hz). Correlation to the 5Me series was helpful: treatment of **13** with DAST at low temperature followed by weak basic workup yielded two crystalline compounds after silica chromatography in 55% and 32% yield (Figure 2b). Single-crystal X-ray diffraction of both structures identified the major product as **31**, an unexpected fragmentation product, and the minor product as 6F,12F-5MePXN (**30**). The ^{19}F coupling constant of **30** was found to be 27.8 Hz, aiding the assignment of **28** via the relationship between C6-F and C12-F. The additional C5-methyl group must significantly stabilize the high-energy, non-classical cation **29**, leading to the unexpected reactivity of decarboxylation and fluoride capture at C3 or C6. The unexpected stabilizing role of the C5-methyl group heralded more remarkable effects in classic solvolytic degradations of PXN.

Picrotoxinin undergoes rapid, reversible hydrolysis to lose efficacy upon storage in water between pH 7–9 or in mouse plasma.[13b] We observed the initial (kinetic) site of hydrolysis with 1 equiv. NaOH to be C11,[26] and exposure to excess base led to complex decomposition.[27] We hypothesized that this latter decomposition derived from irreversible C15 hydrolysis — a "point of no return" due to concomitant epoxide opening or cyclohexane relaxation, with no precedent for chemical or biochemical reversion. Whereas we had previously observed 5-methyl substitution to decrease reversible degradation by halving the pseudo-first order rate constant (D_2O, 8.2 pH*),[28] we had not probed the effect of C5 substitution on irreversible degradation. To our surprise, the effect of C5 methylation was profound.

Warming PXN with 1% H_2SO_4 (0.18 M, aqueous) led to clean conversion to picrotoxic acid (**32**) in 24 hours via cleavage of the C15 lactone, cyclohexane ring-opening and intramolecular

epoxide addition (Figure 3a, top).[6] 5MePXN, in contrast, did not react at all under identical conditions!

Addition of 5 mol% NaOMe to a solution of PXN (**1**) in d_4-methanol at 22 °C led to an equimolar mixture of d_5-methyl picrotoxate (d_5-**33**) and d_9-dimethyl picrotoxinin dicarboxylate (d_9-**34**) in 6 hours (Figure 3a, bottom). In contrast, we did not observe any consumption of 5MePXN under the same conditions (Figure 3b). To ensure an NMR-inactive acidic impurity was not consuming the catalytic strong base, we prepared a 1:1 mixture of PXN and 5MePXN and added 5 mol% NaOMe so that both substrates were exposed to identical conditions: PXN completely degraded, whereas 5MePXN completely persisted (Figure 3c and d). Even addition of 2 equivalents NaOMe had no effect on 5MePXN (Figure 3b and SI), far exceeding the tolerance of PXN. Thus, C5 methylation stabilized PXN against buffered basic water hydrolysis, acidic hydrolysis and alkaline methanolysis (Figure 3a–d and Ref. 14).

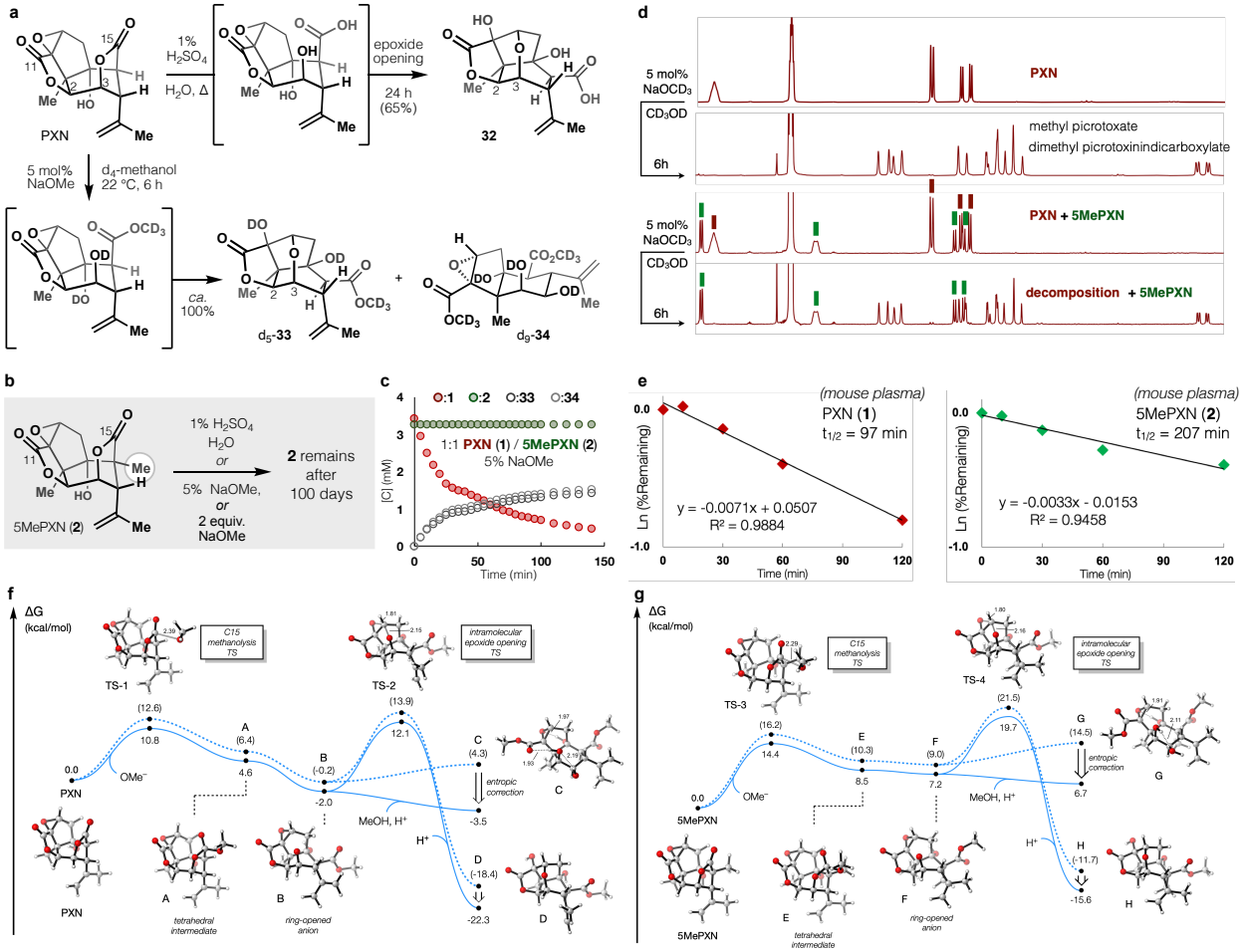

Fig. 3. Experimental and computational analysis of extreme stability imparted by C5-methylation. a. Degradation of **1** using common acidic and basic conditions; **b.** Attempted degradation of 5MePXN (**2**) using the same conditions; **c**. In situ ^{1}H NMR monitoring of 1:1 PXN/ 5MePXN in 5% NaOMe/ d_4-methanol; **d**. Competition experiments with **1** and **2** using 5% NaOMe in d_4-methanol; t = 0 and 6 h, w/ and w/o **2**; **e**. Degradation is also retarded in plasma. **f**. & **g**. Calculated structures and free energies of transition states and intermediates for base-catalyzed methanolysis at the ωB97X-D/def2-TZVPPD, SMD (H_2O)// ωB97X-D/def2-SVP, SMD (H_2O) level of theory. Interatomic distances are in Å. Dashed curves denote raw calculated values; solid curves denote values with translational entropy corrections accounting for concentration gradients (see Supporting Information).

Computational models for stability and affinity. The structural basis for resistance to solvolysis was probed with density functional theory (DFT) computational models to weigh three competing hypotheses: 1) a high barrier to nucleophile addition due to C5Me obstruction of Bürgi-Dunitz[29] or Heathcock's Flippin-Lodge[30] angles; 2) a high barrier to conformational change in methanolysis intermediates; or 3) a high barrier to subsequent reaction of the initial methanolysis product (i.e. formation of 5Me-**33** or 5Me-**34**). Structures and free energies of transition states and intermediates for base-catalyzed methanolysis were calculated at the ωB97X-D/def2-TZVPPD, SMD (H2O)// ωB97X-D/def2-SVP, SMD (H2O) level of theory in Gaussian 16. Comparison of relative energies of intermediateas and transition states of PXN (**1**) and 5MePXN **(2)** solvolyses suggested that the resistance of **2** to methanolysis was unlikely to be caused by kinetic factors (hypotheses #1 and #2) and more likely due to thermodynamic factors (Figure 3f and g). Whereas the C15 methanolysis of **1** to anion **B** could be reversed, epoxide opening (to **C**) and C11 lactone opening (to **D**) provide competitive "escape pathways" for **B** (14.1 kcal/mol barrier to product, 12.8 kcal/mol barrier to starting material). In contrast, calculated energies of the analogous C5Me intermediates reside on a high plateau above **2**; reversion to **2** encounters only a 5.9 kcal/mol barrier, whereas the "escape pathway" to epoxide-opened product **H** requires 12.5 kcal/mol and an overall 19.7 kcal/mol rate-determining step. The 7.4 kcal/mol difference between the intramolecular epoxide opening barriers for picrotoxinin and 5-Me-picrotoxinin roughly translates to a 1.6×10^5-fold difference in rate, in good agreement with the experimental observation that 5-Me-picrotoxinin resists methanolysis.

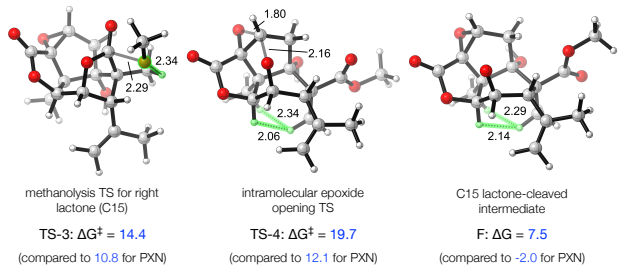

Fig. 4. Relevant interactions with C5Me. Although C5Me clashes with the incoming MeO- nucleophile, the kinetically-relevant effects appear to be diaxial interactions in high-energy twist-boat intermediates.

The major steric interactions that raise the energies of **TS-3** and **TS-4** compared to their picrotoxinin counterparts are shown in Figure **4**. For the nucleophilic attack TS (**TS-3**), the 5-Me substituent clashes directly with the incoming oxygen nucleophile (H...O distance 2.34 Å, or 86% of the sum of the van der Waals radii). For both the C15 lactone-opened intermediates and the intramolecular epoxide opening transition states (**TS-4**), the free energies are raised due to the steric repulsions caused by the pseudoaxial 5-Me group across the cyclohexane ring. Return to the C15 lactone alleviates these repulsive interactions.

Due to the translational potential of these observations, we also investigated the relative rates of hydrolysis observed in mouse plasma. C5 methylation led to a doubling of the extrapolated half-life in plasma (Figure 3e), likely a mixture of reversible C11 hydrolysis[26] and irreversible C15 hydrolysis.[13b] No prior studies have identified PXN modifications that enhance metabolic stability.

LGIC selectivity. The structurally privileged 5-methyl series was assayed for binding to both $GABA_A$ receptors (rat cortex membrane preparations) and RDL (expressed in *Xenopus* oocytes) and compared directly to the parent PXN (C5-H) series. The parallel series of PXN and 5MePXN analogs allowed us to interrogate the idea that dynamic retrosynthetic analysis enables the exploration of advantageous chemical space proximal to a natural product.

The PXN-series (Figure 5a) is plotted in descending order of rat cortex IC_{50} values and correlated with arrows to the corresponding 5Me-analogs. Hydrophobic substitution of C12/C13 ($-CH_2-$, $-CH_3$) maintained potency, whereas polar substitution (-OH, -F) reduced potency and alkene hydrogenation lay somewhere in between. Among the more potent compounds, we found

that replacement of the C6 hydroxyl with fluoride had little effect on potency as did deoxygenation of the C8,9-epoxide. The least potent analogs included the natural product PTN and its 6F-analog, providing a series that spanned almost 3 orders of magnitude of potency.

C5-methylation had little effect on the pattern of relative potencies in the series, i.e. 5MePXN recapitulated the SAR for $GABA_A$ receptor binding albeit at lower potency. More important, however, was the contrast between $GABA_A$ and RDL patterns: the 5MePXN series did *not* follow the same relative potencies of PXN analogs at the RDL receptor. Instead of mirroring the $GABA_AR$ potency trends, C5-methylation increased the RDL potency of 6F and 6F12FPXN, as well as 6FPTN, leading to a ≥200X selectivity index between vertebrate and invertebrate receptors and potency at RDL that slightly exceeded that of PXN itself. 6FPXN had been reported previously to lose channel blocking ability.[25] Whereas the complex picrotoxane member picrodendrin O has shown high RDL affinity, its selectivity derives from a complex ring at C9 and leads to only a 76-fold selectivity index over $GABA_A$.[31] Its isolation yield of 400 ppb limits its potential.[32] In contrast, selectivity in this 5MePXN series derives from simple core modifications and accompanies high scaffold stability. These are the first assays of PXN analogs generated by total synthesis[24] and the only LGIC-selective PXN analogs reported to date.[33]

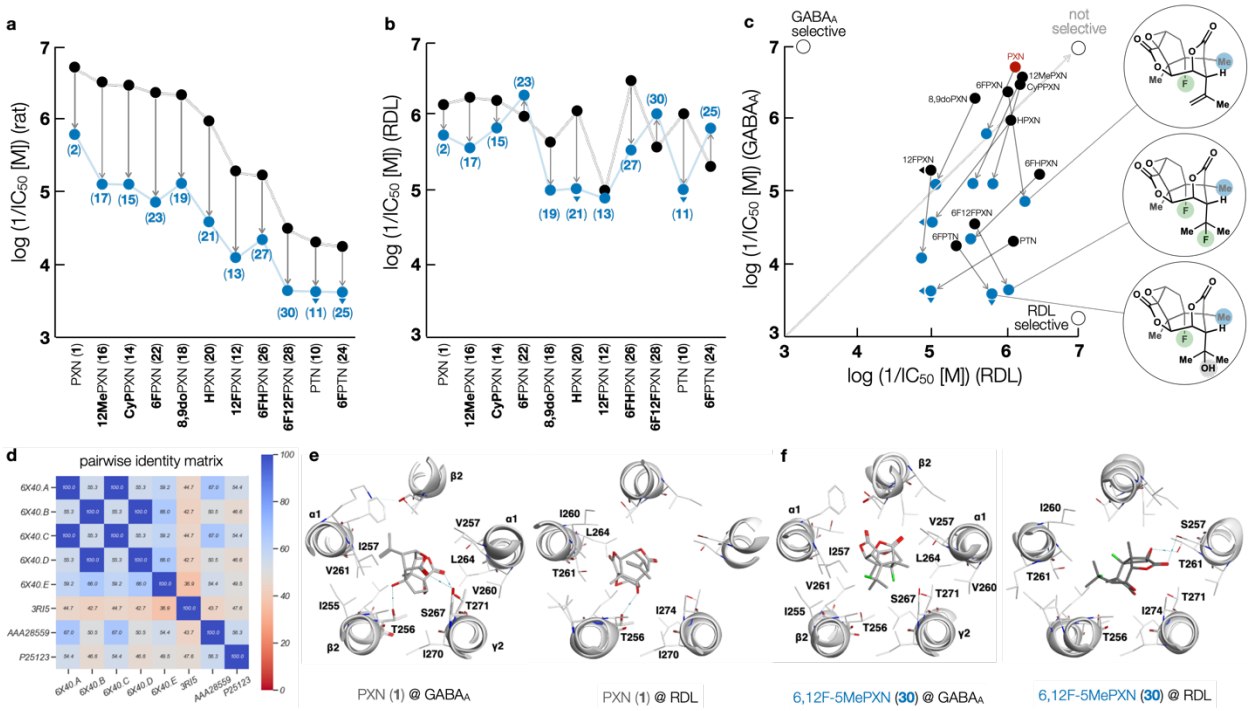

Fig. 5. Experimental and computational analysis of LGIC binding and selectivity. **a,** Relative potencies of PXN (•) and 5MePXN (•) analogs at $GABA_AR$ ([^{3}H]-TBOB). **b,** Relative potencies of PXN (•) and 5MePXN (•) analogs at RDL receptors measured by electrophysiology; **c,** Selectivity between vertebrate ($GABA_A$) and invertebrate (RDL) receptors by PXN analogs: C5-methylated analogs are selective for invertebrate receptors. **d,** Pairwise identity matrix of GABA/RDL residues across species. **e,** Best binding poses of PXN (**1**) in *R. norvegicus* $GABA_A$ and *D. melanogaster* RDL, as predicted from molecular dynamics (MD) simulations. The binding free energy of **30** is predicted to be 1.8 ± 1.5 kcal/mol above that of **1** at $GABA_A$. Orientation of the binding pocket is kept fixed to allow direct comparison of binding poses. **f,** Best binding poses of (**30**) in *R. norvegicus* $GABA_A$ and *D. melanogaster* RDL, as predicted from molecular dynamics (MD) simulations.

Computational binding models. To probe the basis for selectivity of **30** (6,12-difluoro-5-methyl-PXN) for RDL and against $GABA_A$ we constructed *in silico* models using literature coordinates.[34] The helical region of human $GABA_A$ with picrotoxinin bound (PDB 6X40) was used as a template

structure to build homology models of GABA in *R. norvegicus* and RDL in *D. melanogaster*. Two sequences of the β-unit in *D. melanogaster* RDL (NCBI AAA28559, UniProt P25123) were analyzed for similarity to the template structure. The NCBI sequence was used to build the RDL model due to greater homology with each chain of the template structure. Protein structures were prepared, and protonation issues were fixed using Structure Preparation in MOE (for a full description of computational modeling building and refinement, see the SI).

Refined models of $GABA_A$ identified a pose for PXN similar to the pose modeled to electron density of PXN within a GluCl-Fab-ivermectin crystal at 3.3 Å resolution,[16] where the isopropenyl substituent is directed to the cytosolic exit (opposite to the pose ascribed to the electron density in a recent CryoEM structure of a full-length α1β3γ2L $GABA_A$ receptor with PXN bound at its pore).[17] Similar to both structures, PXN is encircled between the 2' and 9' residues and the C11/C15 carbonyl oxygens accept hydrogen bonds from sidechain alcohols of S267 and T271 in the γ2 helix (Figure 6e, left). An additional interaction is observed between the PXN C6 alcohol and the sidechain of T256 in a nearby β2 helix. The latter interaction is observed in the fly RDL model, illuminating the similar potency of PXN in both organisms (Figure 6e, right).

In contrast, the lowest energy binding pose of **30** with the rat $GABA_A$ model rotates away from the S267/T271 hydrogen bond network to accommodate increased steric bulk (Figure 6f, left), leading to weaker binding (see SI). Given the narrow pore size of $GABA_A$ and the increase in overall volume of **30** (247 $Å^3$ vs. 229 $Å^3$), this decreased tolerance is not surprising. The fly RDL model, however, appears to accommodate the steric size of the C12 fluorine and C5 methyl. Additionally, the C11 carbonyl and C7,8 epoxide of **30** interact with the sidechain alcohol groups of S257 and T261, respectively. These interactions of **30**, which are specific to the fly RDL model, help to explain the selectivity of **30** to *D. melanogaster* RDL compared to mammalian $GABA_A$. The general tolerance of RDL to C5 methylation (Figure 6c) compared to $GABA_A$ suggests that other LGICs homologous to RDL may be similarly accommodating.

Despite its long history, picrotoxinin's instability, complexity, and toxicity have discouraged its use in optimization campaigns. Here we show that C5 methylation imparts stability, accessibility, and selectivity. This discovery came from the identification of 5MePXN as a target of convenience during recursive retrosynthetic analyses and synthetic studies toward PXN itself.[14] We find that 5MePXN, in addition to being conveniently accessed, holds many attributes that surpass those of PXN, including higher complexity, which has been correlated to higher average selectivity among diverse proteins.[35] In contrast to both traditional total synthesis and scaffold-hopping FOS, dynamic retrosynthesis alters the target during analysis, but maintains most physicochemical properties of the target itself. We hope this strategy will enable many natural products to be studied, improved, and leveraged against important targets. The 5MePXN series of "supernatural products"[36] might be best brought to bear on infectious disease if the affinity towards GluCl receptors can be increased.[16] This work is ongoing.

Acknowledgements. Dr. Milan Gembicky, Dr. Erika Samolova, Dr. Jake Bailey, Professor Arnold Rheingold and the UCSD Crystallography Facility are acknowledged for X-ray crystallographic analysis. Dr. Laura Pasternack and Dr. Dee-Hua Huang are acknowledged for assistance with NMR spectroscopy. Support was provided by the National Institutes of Health (R35 GM122606) and JITRI (Fellowship to G.T.).

Author contributions. R.A.S., G.T., J.W. and Z.B. conceived the project. R.A.S. directed the research and composed the manuscript, and G.T. compiled the Supporting Information section. G.T. executed all synthetic and spectroscopic work, S.G. and K.B. undertook electrophysiology on RDL, S.C. and A.C. contributed the computational analyses of reaction coordinates in Fig. 3 and 4, and A.S. contributed the computational binding studies in Fig. 5.

Data and materials availability:
All data are available in the main text or Supplementary Information.

Code Availability:
Crystallographic data are available from the Cambridge Crystallographic Data Centre (CCDC) under the following reference numbers: CCDC2048201 (**11**), CCDC2081332 (**13**), CCDC2071501 (**14**), CCDC2048202 (**20**), CCDC2048203 (**20**), CCDC2069870 (**23**), CCDC2079783 (**30**), CCDC2078168 (**31**), CCDC2087432 (d_9-**34**).

References

1. Boger, D. L. The difference a single atom can make: synthesis and design at the chemistry–biology interface. *J. Org. Chem*. **82**, 11961–11980 (2017).
2. Wender, P. A., Verma, V. A., Paxton, T. J., Pillow, T. H. Function-oriented synthesis, step economy, and drug design. *Acc. Chem. Res.* **41**, 40−49 (2008).
3. Huffman, B. J.; Shenvi, R. A. Natural products in the "marketplace": interfacing synthesis and biology *J. Am. Chem. Soc.* **141**, 3332–3346 (2019).
4. Roach, J. J.; Sasano, Y.; Schmid, C. L.; Zaidi, S.; Katritch, V.; Stevens, R. C.; Bohn, L. M.; Shenvi, R. A. Dynamic strategic bond analysis yields a ten-step synthesis of 20- nor-salvinorin A, a potent κ-OR agonist. *ACS Cent. Sci.* **3**, 1329−1336 (2017).
5. Boullay, P. F. G. Analyse chemique de la coque du levant, menispermum cocculus *Bull. Pharm.* **4**, 1–34 (1812).
6. Porter, L. A. Picrotoxinin and related substances *Chem. Rev.* **67**, 441 (1967).
7. (a) Van der Kloot, W. G., Robbins, J. The effects of γ-aminobutyric acid and picrotoxin on the junctional potential and the contraction of crayfish muscle. *Experientia* **15**, 35–36 (1959); (b) Jarboe, C. H., Porter, L. A., Buckler, R. T. Structural aspects of picrotoxinin action. *J. Med. Chem.* **11**, 729–731 (1968). (c) Farrant, M. I, Webster, R. A. GABA antagonists, their use and mechanisms of action. *Neuromethods*, 1989, vol. 12: Drugs as Tools in Neurotransmitter Research, ed. Boulton, A. B., Baker, G. B.; Juorio, A. V., pp. 161-219. Humana Press, New Jersey.
8. Barth, L.; Kretschy, M. Zur Picrotoxinfrage. *Monatshefte fuer Chemie*, **2**, 796–809 (1884).
9. (a) Olsen, R. W., Sieghart, W. International union of pharmacology. LXX. Subtypes of γ-aminobutyric acid A receptors: classification on the basis of subunit composition, pharmacology, and function. Update *Pharmacol. Rev.* **60**, 243–260 (2008); (b) Johnston, G. A. R. Advantages of an antagonist: bicuculline and other GABA antagonists. *Br. J. Pharm.*, **169**, 328–336 (2013).
10. Jaiteh, M., Taly, A., Hénin, J. Evolution of pentameric ligand-gated ion channels: pro-loop receptors. *PLoS ONE*, **11**, e0151934 (2016).
11. Burkhill, P. I., Holker, J. S. E., Robertson, A., Taylor, J. H. Picrotoxin. Part VI.* Picrotoxic acid and its derivatives. *J. Chem. Soc.*, 4945–4952 (1957).
12. Horrmann, P. Beiträge zur Kenntnis des Pikrotoxins. *Justus Liebigs Ann. Chem.* **411**, 273–314 (1916).

13. (a) Ramwell, P. W., Shaw, J. E. Some observations on the physical and pharmacological properties of picrotoxin solutions. *J. Pharmacy Pharmacol.*, *15*, 611–619 (1963); (b) Pressly, B. Vasylieva, N., Barnych, B., Singh V., Singh, L., Bruun, D. A., Hwang, S. H., Chen, Y.-J., Fettinger, J. C., Johnnides, S., Lein, P. J.; Yang, J., Hammock, B. D., Wulff, H. Comparison of the toxicokinetics of the convulsants picrotoxinin and tetramethylenedisulfotetramine (TETS) in mice. *Archives Tox.* **94**, 1995–2007 (2020).
14. Crossley, S. W. M.; Tong, G.; Lambrecht, M.; Burdge, H. E.; Shenvi, R. A. Synthesis of picrotoxinin via late-stage strong bond activations. *J. Am. Chem. Soc.* **142**, 11376–11381 (2020).
15. Gielen, M.; Thomas, P.; Smart, T. G. The desensitization gate of inhibitory Cys-loop receptors. *Nature Comm. 6*, 6829 (2015).
16. Hibbs, R. E.; Gouaux, E. Principles of activation and permeation in an anion-selective Cys-loop receptor. *Nature* **474**, 54–60 (2011).
17. Masiulis, S., Desai, R., Uchanski, T., Serna Martin, I., Laverty, D., Karia, D., Malinauskas, T., Zivanov, J., Pardon, E., Kotecha, A., Steyaert, J., Miller, K. W., Aricescu, A. R. $GABA_A$ receptor signaling mechanisms revealed by structural pharmacology. *Nature* **565**, 454–459 (2019).
18. Ref. 14 estimated an IC_{50} of 9 μM, but this value has been refined.
19. (a) Crossley, S. W. M.; Obradors, C.; Martinez, R. M.; Shenvi R. A. Mn-, Fe-, and Co-catalyzed radical hydrofunctionalizations of olefins. *Chem. Rev.* **116**, 8912–9000 (2016). (b) Green, S. A.; Crossley, S. W. M.; Matos, J. L. M.; Vásquez-Céspedes, S.; Shevick, S. L.; Shenvi, R. A. The high chemofidelity of metal-catalyzed hydrogen atom transfer. *Acc. Chem. Res.* **51**, 2628–2640 (2018).
20. Barker, T. J.; Boger, D. L. Fe(III)/$NaBH_4$-mediated free radical hydrofluorination of unactivated alkenes. *J. Am. Chem. Soc.* **134**, 13588–13591 (2012).
21. Denmark, S. E., Edwards, J. P. A comparison of (chloromethyl)- and (iodomethyl)zinc cyclopropanation reagents. *J. Org. Chem.* **56**, 6974–6981 (1991).
22. Huang, S.H.; Duke, R.K.; Chebib, M.; Sasaki, K.; Wada, K.; Johnston, G.A.R. Bilobalide, a sesquiterpene trilactone from Ginkgo biloba, is an antagonist at recombinant α1β2γ2L $GABA_A$ receptors. *Eur. J. Pharmacol.* **464**, 1–8 (2003).
23. (a) Dao, H. T., Li, C., Michaudel, Q., Maxwell, B. D., Baran, P. S. Hydromethylation of unactivated olefins. *J. Am. Chem. Soc.* **137**, 8046–8049 (2015). (b) Green, S. A.; Huffman, T. R.; McCourt, R. O.; van der Puyl, V.; Shenvi, R. A. Hydroalkylation of olefins to form quaternary carbons. *J. Am. Chem. Soc.* **141**, 7709–7714 (2019).
24. Krische, M. J.; Trost, B. M. Transformations of the picrotoxanes: the synthesis of corianin and structural analogues from picrotoxinin. *Tetrahedron* **54**, 7109 (1998).
25. Shirai, Y.; Hosie, A. M.; Buckingham, S. D.; Holyoke, C. W.; Baylis, H. A.; Sattelle, D. B. Actions of picrotoxinin analogues on an expressed, homo-oligomeric GABA receptor of *Drosophila melanogaster*. *Neurosci. Lett.* **189**, 1 (1995).
26. Tong, G.; Shenvi, R. A. Revision of the unstable picrotoxinin hydrolysis product. *Angew. Chem. Int. Ed.* **60**, 19113 (2021).
27. (a) Conroy, H. Picrotoxin. V. Conformational analysis and problems of structure. *J. Am. Chem. Soc.* **79**, 5550–5553 (1957); (b) Burkhill, P. I.; Holker, J. S. E.; Robertson, A.; Taylor, J. H. Picrotoxin. Part VI. Picrotoxic acid and its derivatives. *J. Chem. Soc.* 4945 (**1957**); c) Conroy, H. Picrotoxin. I. The skeleton of picrotoxinin. The degradation to picrotoxadiene. *J. Am. Chem. Soc.* **74**, 491–498 (1952); d) Horrmann, P. Über Derivate des α- und β-Brompikrotoxinins. *Ber. Dtsch. Chem. Ges.* **46**, 2793 (1913); e) Burkhill, P. I.; Holker, J. S. E. Picrotoxin. Part VIII. The structures of α- and β-picrotoxinones. *J. Chem. Soc.* 4011 (1960).

28. Krężel, A. Bal, W. A formula for correlating pK_a values determined in D_2O and H_2O. *J. Inorg. Biochem.* **98**, 161 (2004).
29. Bürgi, H. B., Dunitz, J. B., Lehn, J. M., Wipff, G. Stereochemistry of reaction paths at carbonyl centres. *Tetrahedron Lett.* **30**, 1563–1572 (1974).
30. (a) Lodge, E. P., Heathcock, C. H. Steric effects, as well as σ*-orbital energies, are important in diastereoface differentiation in additions to chiral aldehydes. *J. Am. Chem. Soc.* **109**, 3353-3361 (1983). (b) Heathcock, C. H.; Flippin, L. A. Acyclic stereoselection. 16. High diastereofacial selectivity in Lewis acid mediated additions of enol silanes to chiral aldehydes. *J. Am. Chem. Soc.*, **105**, 1667–1668 (1983).
31. Hosie, A. M.; Ozoe, Y.; Koike, K.; Ohmoto, T.; Nikaido, T.; Sattelle, D. B. Actions of picrodendrin antagonists on dieldrin-sensitive and -resistant *Drosophila* GABA receptors. *Brit. J. Pharmacol.* **119**, 1569–1576 (1996).
32. Suzuki, Y.; Koike, K.; Ohmoto, T. Eight picrotoxane terpenoids, picrodendrins K–R, from *Picrodendron baccatum. Phytochem.* **31**, 2059–2064 (1992).
33. For RDL selective natural products within the picrotoxane series, see: Ozoe, Y.; Akamitsu, M.; Higata, T.; Ikeda, I.; Mochida, K.; Koike, K.; Ohmoto, T.; Tamotsu, N. Picrodendrin and related terpenoid antagonists reveal structural differences between ionotropic GABA receptors of mammals and insects. *Bioorg. Med. Chem.* **6**, 481–492 (1998).
34. Kim, J. J.; Gharpure, A.; Teng, J.; Zhuange, Y.; Howard, R. J.; Zhu, S.; Noviello, C. M.; Walsh Jr., R. M.; Lindahl, E.; Hibbs, R. E. Shared structural mechanisms of general anaesthetics and benzodiazepines. *Nature* **585**, 303-308 (2020).
35. Clemons, P. A.; Bodycombe, N. E.; Carrinski, H. A.; Wilson, J. A.; Shamji, A. F.; Wagner, B. K.; Koehler, A. N.; Schreiber, S. L. Small molecules of different origins have distinct distributions of structural complexity that correlate with protein-binding profiles. *Proc. Natl. Acad. Sci. U. S. A.* **107**, 18787−18792 (2010).
36. (a) Wu, Z.-C.; Boger, D. L. The quest for supernatural products: the impact of total synthesis in complex natural products medicinal chemistry. *Nat. Prod. Rep.* **37**, 1511–1531 (2020); (b) Wan, K. K.; Shenvi, R. A. Conjuring a supernatural product – DelMarine. *Synlett*, **27**, 1145–1164 (2016).